Computational Simulation of Two-dimensional Turbulent Film Cooling, Using LES Approach and Considering Density Ratio Effects

M. Ramezanizadeh[1, a], M.H. Saidi[2,a], and M. Taeibi-Rahni[3,a,b]
a-Mech. Eng. Dep't. b-Aerospace Eng. Dep't.
Sharif University of Technology

ABSTRACT
Film cooling of a two-dimensional flat plate at different jet to cross flow velocity ratios (R) is simulated at the jet Reynolds number of 4700, using large eddy simulation (LES) approach. Our computational methodology includes the use of finite volume method, applying the unsteady SIMPLE algorithm and a multi-block and non-uniform staggered grid. The governing equations have been discretized applying the Power-Law scheme for the spatial terms and the Crank-Nicolson scheme for the temporal terms. Two solution approaches are discussed here, namely:1-neglecting and 2-considering density ratio effects. The results showed that the density ratio has significant effects on the flow structures, namely on the penetration, the expansion, and the reattachment point of the vortical regions. Therefore, it changes the temperature distribution and the film cooling effectiveness, and thus, it should not be easily neglected.

Key Words: Large Eddy Simulation (LES), Film Cooling Effectiveness, Density Ratio, Jet into Cross Flow

شبیه سازی عددی خنک کاری لایه ای آشفته دو بعدی، با استفاده از رهیافت LES و با در نظر گرفتن اثر نسبت چگالی

مهدی رمضانی زاده [a,۱] محمدحسن سعیدی [a,۲] محمد طیبی رهنی [b ,a,۳]
a-دانشکده مهندسی مکانیک b-دانشکده مهندسی هوافضا
دانشگاه صنعتی شریف

چکیده
در این تحقیق، خنک کاری لایه ای صفحه تخت دوبعدی در نسبت سرعت های مختلف در عدد رینولدز ۴۷۰۰، با استفاده از روش شبیه سازی گردابه های بزرگ مطالعه شده است. روش عددی بکار رفته شامل روش حجم محدود، الگوریتم غیر دائم سیمپل و شبکه چند بلوکی غیر یکنواخت جابجا شده می باشد. معادلات حاکم با استفاده از روش قانون توانی برای عبارت های مکانی و روش کرانک- نیکلسون برای عبارت های زمانی گسسته سازی شده اند. دو رهیافت حل، شامل صرفنظر کردن و در نظر گرفتن اثرات نسبت چگالی به کار گرفته شده است. نتایج حاصل نشان می دهد که تغییرات نسبت چگالی اثرات مهمی بر ساختارهای جریان، شامل نفوذ، انبساط و نقطه تماس مجدد نواحی چرخشی دارد که توزیع دما و اثربخشی خنک کاری لایه ای را تغییر می دهد. لذا، اثرات نسبت چگالی به راحتی قابل صرفنظر کردن نمی باشند.

واژه های کلیدی: رهیافت شبیه سازی گردابه های بزرگ، اثربخشی خنک کاری لایه ای، نسبت چگالی، جریان جت در جریان عرضی

1. Phd Student (Crresponding Auther): ramezanizadeh@mehr.sharif.edu
2. Associate Professor: saman@sharif.edu
3. Associate Professor: taeibi@sharif.edu

Numenclature

C_S	Smagorinsky Subgrid Scale Stress Model Coefficient
D	Jet hydraulic Diameter
l	Characteristic Length Scale
P	Pressure
Pr	Molecular Prandtl Number
Pr_t	Turbulent Prandtl Number
q_i	Subgrid Scale Heat Flux ($\equiv \overline{\rho}(u_i T - \widetilde{u}_i \widetilde{T})$)
R	Jet to Cross Flow Velocity Ratio
Re	Reynolds Number
S	Sutherland Parameter ($\equiv 110.4/T_{ref}$)
$\overline{S_{ij}}$	Resolved Strain Rate Tensor ($\equiv \left(\partial\overline{u}_i/\partial x_j + \partial\overline{u}_j/\partial x_i\right)/2$)
t	Time
T	Temperature
T_{ref}	Reference Temperature
T_{aw}	Adiabatic Wall Temperature
u, v	Velocity Components in the X- and Y-Directions, Respectively
u_i	Velocity Components in x_i Directions
$\overline{u}_i$	Resolved Velocity Components in x_i Directions
x, y, z	Cartesian Coordinates
x_i	Tensor Coordinates, i=1 or 2 for X or Y.

Abbreviations

∞	Farfield or Infinity
sgs	Subgrid Scale
i, j, k	Directions
jet	Directions

Greek Symbols

Δ	Grid Size
$\overline{\Delta}$	Filter Width
Δt	Time Step
α	Kolmogorov Constant
α_t	Subgrid Scale Eddy Diffusivity
δ_{ij}	Kronecker's Delta
η_{ad}	Adiabatic Film Cooling Effectiveness
μ	Molecular Viscosity
υ_t	Smagorinsky Turbulent Viscosity
ρ	Density
σ_{ij}	Viscous Stress Tensor
τ_{ij}	Subgrid Stress Tensor at the Grid Filter Level
∂_t	Time Derivative
∂_i	Spatial Derivatives in the x_i Directions
$k-\omega$	Turbulence Model

Subscripts

DNS	Direct Numerical Simulation
LES	Large Eddy Simulation
RMS	Root Mean Square
SGS	Subgrid Stress
SST	Shear-Stress Transport

Other Operators

_	Filtered Parameter
< >	Spatial Averaging

1. INTRODUCTION

One of the most powerful means of achieving higher thermal efficiency in gas turbines is increasing the turbine inlet temperature, provided that the turbine blades stay beyond its limiting temperature. To conform this, turbine blades should be cooled efficiently. Several cooling mechanisms are proposed for cooling the turbine blades, namely, impingement cooling of leading edge, convective internal cooling, aspiration cooling, and film cooling. Among these, film cooling is known to be the most efficient mechanism.

In film cooling, cold air is bled from the compressor, canalized into the internal chambers of the cooling blades, and discharged through a series of small holes inclined to the surface. This air provides a thin, cold, and insulating blanket along the external surface of the turbine blade. The task of the blade designer is to achieve optimum cooling by a minimum amount of cooling air used and satisfying blade stress criteria.

So far, in comparison to unit density ratio, not many researchers have investigated the effects of density ratio for such flow computationally. Theodoris et al. [1] studied film cooling injection of coolant air from a showerhead injection system at the leading edge of a high-pressure turbine blade, using a fully implicit three-dimensional finite-volume method on multi-block grid. They compared their

computational results for velocity and pressure fields and turbulence intensity with the experimental results of Ardey [2] for blowing ratio of 0.0, 0.7, and 1.1. Theodoris et al. reported that the standard k-ε turbulence model with wall function is capable of capturing the major details of the flow field including the injection-induced secondary flow vortices, particularly on the suction side as well. But, on the pressure side, the lateral jet spreading is under-predicted somewhat together with an exaggeration of the near-wall sink-wall vortices. On this side, with convex walls, where turbulence anisotropy is appreciable (based on the experiments), fairly better predictions were obtained with anisotropy correction of Bergeles et al. [3] promoting the Reynolds stress in the lateral direction. The correction proposed by Bergeles et al. [3] has no beneficial effect on the suction side with concave walls where the turbulence anisotropy was observed to be much smaller.

Lin and Shih [4] studied the three-dimensional flow and heat transfer about a semi-cylindrical leading edge with a flat after-body that is cooled by film-cooling jets, injected from a plenum through three staggered rows of compound-angle holes. They used the $k-\omega$ shear-stress transport (SST) turbulence model. Comparison of their results with experimental data showed that the normal spreading is under-predicted from 20 to 50 percent, the lateral spreading is over-predicted above the surface, but under-predicted on the surface, and the laterally averaged surface effectiveness was well predicted. They concluded that these errors could be attributed to the isotropic turbulence model used, which can not account for the Reynolds stress redistribution, as eddies flatten and approach the wall.

Azzi and Lakehal [5] studied two classes of turbulent models namely anisotropic eddy-viscosity/diffusivity models and explicit algebraic stress models, with respect to their predictive performance in reproducing near-wall flow physics and heat transfer on a flat plate by a row of stream-wise injected jets. They reported that comparison of the obtained results of wall temperature distributions with the experimental one shows that only the anisotropic eddy-viscosity/diffusivity model can correctly predict the span-wise spreading of the temperature field and reduce the strength of the secondary vortices. Also, the wall-cooling effectiveness was found to essentially depend on these two particular flow features. It should be noted that various quadratic and cubic explicit algebraic stress models were used in their calculations.

Roy et al. [6] performed a flat plate film cooling analysis using a Spalart-Allamaras based detached eddy simulation. Their numerical model included an unstructured grid system to resolve the dynamic flow structures on both sides of the plate as well as inside the hole itself. They obtained detailed computation of a single row of 35 degree round holes on a flat plate for blowing and density ratio of unity and two, respectively. They noted that their approach, which makes no assumption of isotropy downstream of the holes, greatly enhances the realistic description of the dynamic mixing processes.

The present authors have investigated this problem from other perspectives, namely, Ramezanizadeh [7] investigated large eddy simulation of film cooling in a turbulent flow over a flat plate. Ramezanizadeh and Taeibi-Rahni [8] studied large eddy simulation of multiple jets in a cross flow using Smagorinsky model. Keimasi and Taeibi-Rahni [9] performed numerical simulation of jets in a cross flow, using different turbulence models. Ramezanizadeh and Taeibi-Rahni [10] studied large eddy simulation of a two-dimensional flat plate film cooling. Finally, Ramezanizadeh et al. [11] investigated large eddy simulation of density ratio effects on two-dimensional film cooling.

In our previous works, the density variation due to temperature difference between jet and the cross flow has not been considered. While, in real film cooling phenomenon, jet and mainstream temperatures and densities are not the same. Therefore, in this research, effects of both jet to cross flow velocity and density ratios on different flow variables, especially on film cooling effectiveness, are investigated, using LES approach.

There are several parameters which affect the film cooling flow behaviors namely, velocity ratio, density ratio, temperature ratio, jet cross section configuration, injection angle, jets spacing in the span-wise direction, and …. In this research, only the effects of velocity and density ratios are investigated and the other parameters are neglected to simplify the problem geometry. Also, in order to compare the obtained results with the experimental data of Ajersch et al., square cross section jets inclined normally into a crossflow are considered.

2. GOVERNING EQUATIONS

The temperature difference between the cooling air and the mainstream hot gas causes considerable density variations, especially near the jet exit. Since

the flow Mach number is assumed to be less than 0.3, incompressible flow is suggested. The assumption of compressible Navier-Stokes equations to simulate the proposed problem causes the number of iterations needed for the code to converge be excessively high. Therefore, in order to account for the density variations, the fluid density is computed using a scalar transport equation along with the momentum and the energy equations. These equations are solved using a pressure based algorithm. Thus, the LES governing equations are as follows, [12]:

$$\frac{\partial \overline{\rho u_i}}{\partial x_i} = 0,$$

$$\frac{\partial \overline{\rho u_i}}{\partial t} + \frac{\partial}{\partial x_j}(\overline{\rho u_i}\,\overline{u}_j) = -\frac{\partial p}{\partial x_i} + \frac{\partial}{\partial x_j}(\sigma_{ij} - \overline{\rho}\tau_{ij}), \quad (1)$$

$$\frac{\partial \overline{\rho T}}{\partial t} + \frac{\partial}{\partial x_i}(\overline{\rho u_i}\,\overline{T}) = \frac{\partial}{\partial x_i}[\frac{\overline{\mu}}{\Pr}\partial_i \overline{T} - \overline{\rho} q_i],$$

where,

$$\sigma_{ij} = \overline{\mu}(\partial_j \overline{u}_i + \partial_i \overline{u}_j - 2/3\partial_k \overline{u}_k \delta_{ij}). \quad (2)$$

The effects of the small scales are present through the SGS stress tensor and the SGS heat flux, respectively, as:

$$\tau_{ij} = (\overline{u_i u_j} - \overline{u}_i \overline{u}_j), \quad (3)$$

$$q_i = (\overline{u_i T} - \overline{u}_i \overline{T}), \quad (4)$$

which require modeling. The large-scale molecular viscosity, $\overline{\mu}$, is assumed to obey Sutherland's law [12 and 13], i.e.,

$$\frac{\overline{\mu}}{\overline{\mu}_\infty} = \overline{T}^{\frac{3}{2}} \frac{1+S}{\overline{T}+S}, \quad (5)$$

with a Sutherland parameter of $S = 110.4/T_{ref}$. It should also be noted that the above equations govern the evolution of the large energy-carrying scales of motion and the effects of the SGS stress tensor and the SGS heat flux should be modeled.

3. SUBGRID SCALE MODEL

The most widely used model in LES approach was suggested by Smagorinsky in 1963. This model which was later named as Smagorinsky model is based on Boussinesq's approximation, in which the anisotropic part of the SGS stress tensor is related to the strain rate tensor of the resolved fields through an eddy-viscosity coefficient [14], i.e.,

$$\tau_{ij} - \frac{\delta_{ij}}{3}\tau_{kk} = -2\nu_t \overline{S}_{ij}, \quad (6)$$

where, ν_t is the eddy viscosity. This quantity is computed from the resolved strain rate tensor magnitude and a characteristic length scale as:

$$\nu_t = l\left|\overline{S}\right| = C_s \overline{\Delta}^2 \left|\overline{S}\right|, \quad (7)$$

where, l is a characteristic length scale and is assumed to be proportional to the filter width ($\overline{\Delta}$) and Smagorinsky coefficient, C_S. Note that $\left|\overline{S}\right|$, is the magnitude of the resolved strain rate tensor, which is defined as:

$$\left|\overline{S}\right| = (2\overline{S}_{ij}\overline{S}_{ij})^{1/2}, \quad (8)$$

and,

$$\overline{S}_{ij} = \frac{1}{2}(\frac{\partial \overline{u}_i}{\partial x_j} + \frac{\partial \overline{u}_j}{\partial x_i}). \quad (9)$$

The, the SGS heat flux is related to the resolved temperature field through SGS eddy diffusivity [15 and 16], i.e.,

$$q_i = -\alpha_t \frac{\partial \overline{T}}{\partial x_i}, \quad (10)$$

and the SGS eddy diffusivity is defined as:

$$\alpha_t = \frac{\nu_t}{\Pr_t}. \quad (11)$$

Note that the Smagorinsky coefficient, C_S, has a range of 0.1 to 0.25 and $\Pr_t = 0.5$ [15].

Lilly [13] showed that under idealized conditions, the Smagorinsky model is consistent with an infinitely extended inertial subrange. Conducting analysis only for an infinitely extended inertial subrange and a cut-off filter, he derived that:

$$C_S = \frac{1}{\pi}(\frac{2}{3\alpha})^{3/4}. \quad (12)$$

Refined theoretical studies for more realistic spectra and other filter functions have not revealed a considerable sensitivity of the value of the Smagorinsky constant. Assuming a Kolmogorov constant of $\alpha = 1.5$, one may find $C_S \approx 0.17$. It should be noted that, in the present work, the Smagorinsky constant is assumed to be 0.17.

4. NUMERICAL METHODOLOGY

The present computational methodology includes a finite volume method, using SIMPLE algorithm, employing a multi-block and non-uniform staggered grid. It should be noted that in the interface of the two blocks of crossflow and jet flow, the grid points are located exactly in the same locations. A power-law differencing scheme is used for the convective and diffusive terms and the Crank-Nicolson scheme is applied for the time discretization. It should be noted that the computational domain and its boundary conditions are selected based on the experimental and computational work of Ajersch et al. [17], which is used as one of our benchmarks. However, our investigations are performed in a two-dimensional domain, considering jet to cross flow

temperature and density ratios effects, while they had assumed no differences between jet and cross flow temperatures and densities. A 1/7 power law velocity profile is considered at the cross flow inlet, where uniform flow at the jet inlet is used. Also, uniform time step of $\Delta t = 0.01$ is considered for time marching to t = 70 second. Note that we have used the time averages of the results for the present work for our investigations.

4.1. CODE DEVELOPMENT and BENCHMARKING

Considering the above computational methodologies, here, three versions of LES code have been developed for the simulations, namely 2-D and 3-D both incompressible and 2-D compressible versions. Primarily, the 2-D incompressible version of the code was developed which was applied to study the first case, i.e., neglecting the density variation in film cooling. Then, the code was upgraded, adding the capabilities to simulate the density variation effects. Later on, the 2-D incompressible version of the code was extended to 3-D.

Benchmarking was pursued considering three different cases, namely two- and three-dimensional cavity flow and three-dimensional multiple jets in a cross flow, using 2- and 3-D versions of the developed code. First, 2-D incompressible flow in a square Cavity at Re=1000 was simulated and the results were compared with the bench mark (DNS) results of Ghia and Ghia [18]. More details in this regard can be found in Ramezanizadeh [7].

Second, time-dependent incompressible flow in a 3-D cavity was simulated at two different Reynolds numbers including 3,200 and 10,000. Time-averaged profiles of mean velocities, root-mean-square (RMS) velocities and Reynolds stresses were computed at the centerlines of the cavity and were compared with the experimental data of Prasad and Koseff [19]. The obtained results show good agreements with the experimental ones. More details of the aforementioned investigation can be found in Taeibi-Rahni and Ramezanizadeh [20].

Third, 3-D incompressible multiple jets in a cross flow at three different velocity ratios, including 0.5, 1.0 and 1.5, were simulated at Re=4700. The mean velocity profiles at different X-positions after the jet exit at Z=0.0 plane were compared with the experimental measurements and the computational results of $k-\varepsilon$ turbulence modeling of Ajersch et al. [17]. The LES results showed much better agreements with the experimental measurements of Ajersch et al. [17], in comparison with their own computational results. More details in this regard can be found in Ramezanizadeh and Taeibi-Rahni [8].

4.2. CONFIGURATION, GRID, and BOUNDARY TREATMENTS

Due to the interactions of the discharged jet and the cross flow, the flow in the vicinity of the film-cooling discharge hole is quite complex. In this work, the simulation is performed using three different velocity ratios, namely, 0.5, 1.0, and 1.5 and a jet Reynolds number of 4700. The jet to cross flow temperature ratio is assumed to be 0.5, which results the jet to cross flow density ratio of 2.0, having ideal gas behavior for both jet and crossflow.

The computational domain and its boundary conditions are shown in Fig. **1.** The coordinate system used is Cartesian (X, Y), where X is aligned with the cross flow direction and Y is perpendicular to the crossflow direction. The origin of the coordinate is located on the geometrical center of the jet exit to the cross flow.

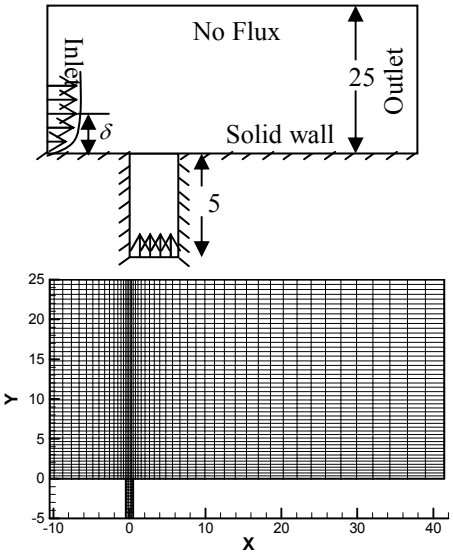

Fig. 1: Physical and computational domains of the 2-D film cooled wall, which are applied for the simulations.

Table 1: Grid arrangements used for grid resolution study.

Block	Grid	Grid Points		Min. Grid Spacing		Max. Grid Spacing	
		X	Y	X	Y	X	Y
Jet Flow	First	6	24	0.2	0.2	0.2	0.24
	Second	21	47	0.05	0.05	0.05	0.11936
	Final	65	161	0.015625	0.015625	0.015625	0.09917
Cross Flow	First	60	90	0.2	0.2	1.856	0.339
	Second	140	180	0.05	0.05	0.926	0.1686
	Final	560	380	0.015625	0.015625	0.2188	0.1184

Grid refinement was performed near the solid walls of Y-direction for both the crossflow and the jet flow blocks. Grid was stretched in the cross flow block near the jet exit in X-direction as well. Grid resolution study and its error estimation were performed applying the Richardson extrapolation method. First, flow was simulated considering two different grid arrangements for unit density flow at R=1.5. Based on the obtained U-velocity profiles at different X-positions after the jet exit, minimum grid spacing near the solid walls were obtained under the Richardson extrapolation method, considering error of 10^{-3}. Therefore, the final grid was constructed for both jet and cross flow blocks. Table **1** shows the specifications of these grid arrangements. The results of U-velocity profiles are shown at different X-positions, namely X=0.0, 5.0, and 10.0, in Fig. **2.**

5. RESULTS

The density ratio effects are investigated in a two-dimensional film cooled wall, using LES approach. Two different cases are investigated. First, the problem is solved neglecting the density variation due to the temperature difference between the jet and the mainstream flows, i.e., any density variations are not considered and only the temperature difference between the jet and the cross flow is considered. Second, the same problem is solved considering the density differences between the jet and the cross flow.

There are several dimensionless parameters affecting the characteristics of such flow. Among these, jet to cross flow velocity and density ratios (R and DR) are studied here.

Since the incoming jet flow direction is normal to the cross flow at all considered velocity ratios, there are two separated regions upstream and downstream of the jet exit, where there are some vortical motions. At all cases, it was observed that the downstream vortical region is unstable and the vortices move towards the downstream boundary. Motion of this vortical region results the time variations of the flow velocity components, pressure and temperature. Figure **3** shows the time history of the U-velocity profiles at an arbitrary point (X=3.0 and Y=1.0) after the jet exit at velocity ratio of 0.5 and density ratios of 1.0 and 2.0.

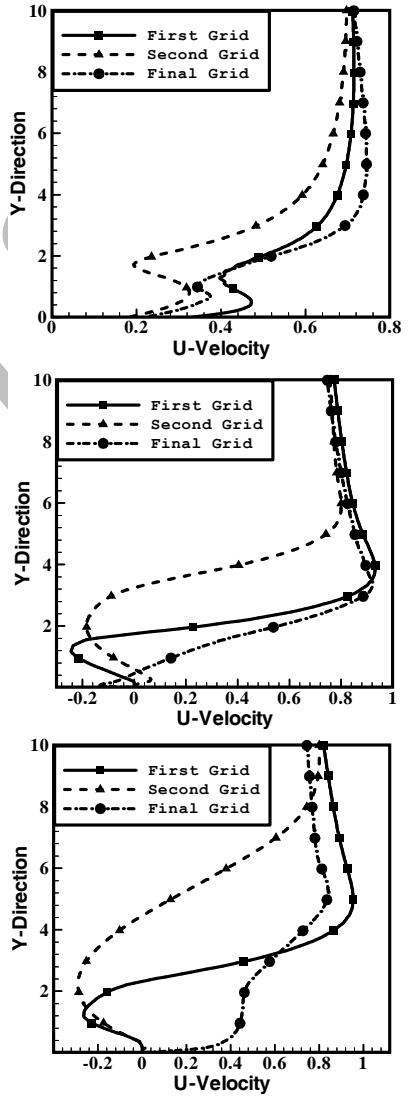

Fig. 2: U-velocity profiles at different X-positions, namely X=0.0, 5.0, and 10.0, applying Richardson extrapolation method.

The time averaged flow streamlines and the temperature contours at different velocity ratios, namely 0.5, 1.0, and 1.5, are shown in Fig.'s **4, 5,** and **6** at both cases, namely neglecting and

considering the density ratio effects. At the right top of the above mentioned streamline Figures, the jet exit regions are zoomed to show the flow features in that regions.

In Fig. **4**, the time averaged flow streamlines and the temperature contours are shown at R=0.5 and at DR=1.0 and 2.0. As it was noted before, when the jet enters the cross flow, two vortical regions are generated upstream and downstream of the jet. The downstream vortical region contains two vortices, while the upstream region contains two vortices at DR=1.0 and one vortex at DR=2.0. The streamlines show that by considering density variation effects, the maximum penetration of the jet flow into the cross flow in Y-direction will be decreased nearly 0.4D. Also, the penetration of the downstream vortical region in X-direction into the cross flow decreases. Therefore, the reattachment point of the downstream vortical region moves approximately 1.6D in X-direction towards the jet exit. On the other hand, considering the density ratio variations, result in lower jet flow penetration in Y-direction and a smaller downstream vortical region. This flow behavior changes the temperature distribution, which is shown as temperature contours in Fig. **4.** That is, considering the density ratio variations; result in lower mixing of the cold jet flow with the hot crossflow.

In Fig. **5**, the time averaged flow streamlines and the temperature contours are shown for R=1.0 and for DR=1.0 and 2.0. The downstream vortical region contains two vortices, while the upstream region contains two vortices at DR=1.0 and one vortex at DR=2.0. Note that by increasing the velocity ratio, the two vortical regions expand in both X- and Y-directions, in comparison with the jet flow into the cross flow in Y-direction would be increased nearly 0.3D

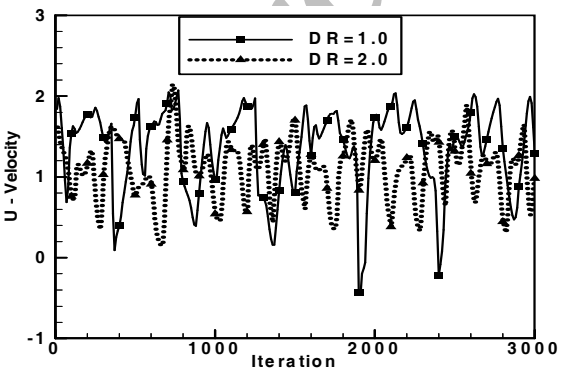

Fig. 3: The time history of the U-velocity profiles at an arbitrary point (X=3.0 and Y=1.0) after the jet exit at R=0.5 and DR=1.0 and 2.0

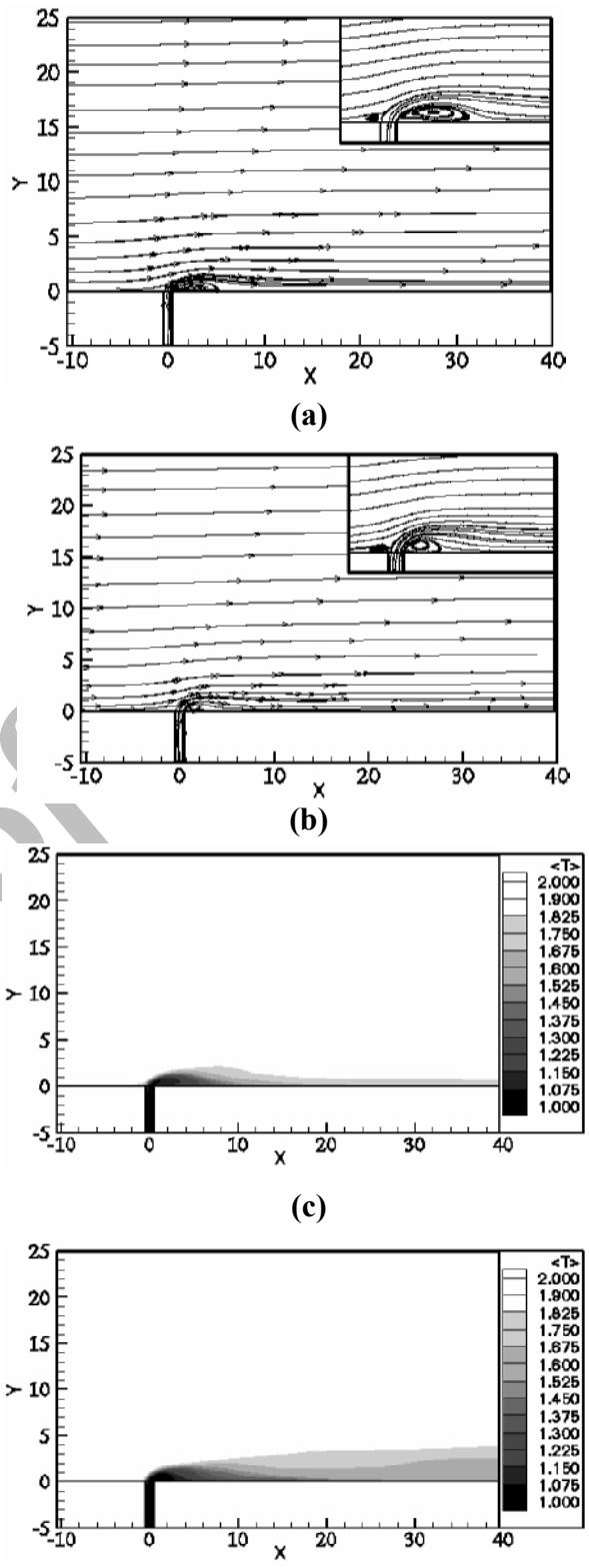

Fig. 4: The flow streamlines and the temperature contours at R=0.5: (a) and (b) Streamlines and (c) and (d) temperature contours at DR=1.0 and 2.0, respectively

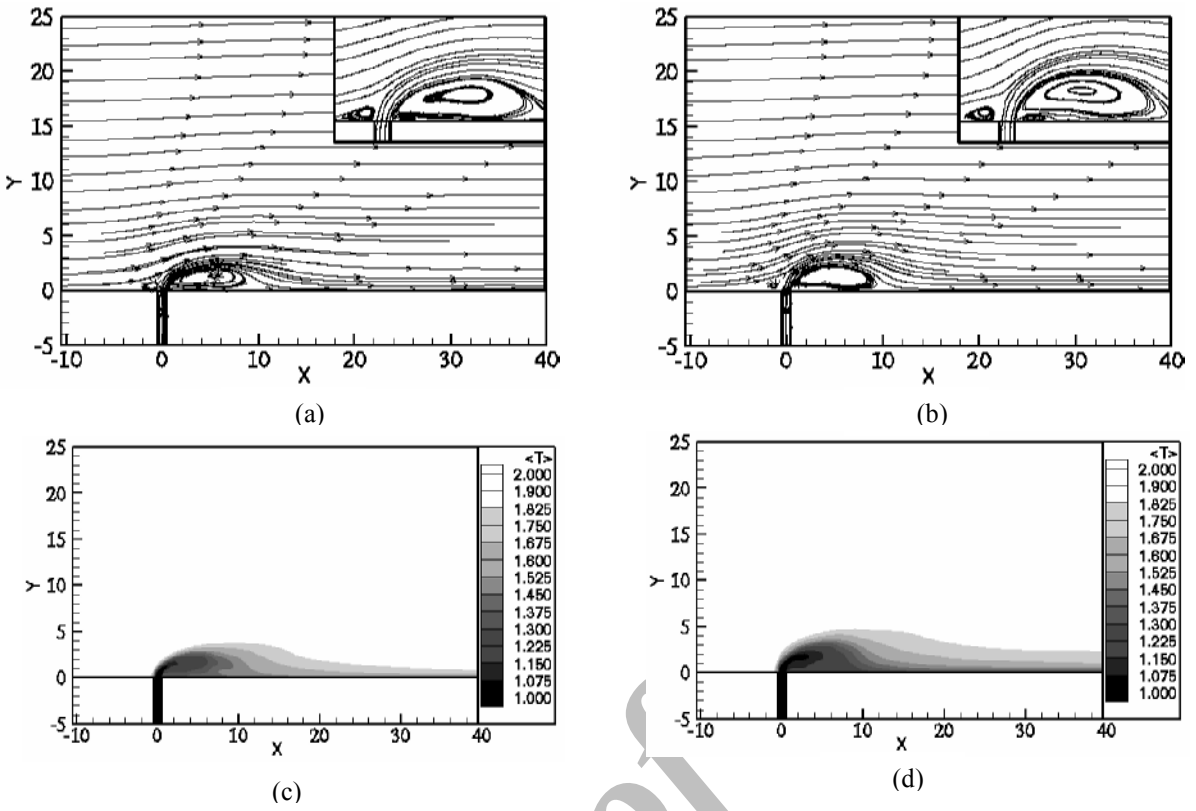

Fig. 5: The flow streamlines and the temperature contours at R=1.0: (a) and (b) Streamlines and (c) and (d) temperature contours at DR=1.0 and 2.0, respectively.

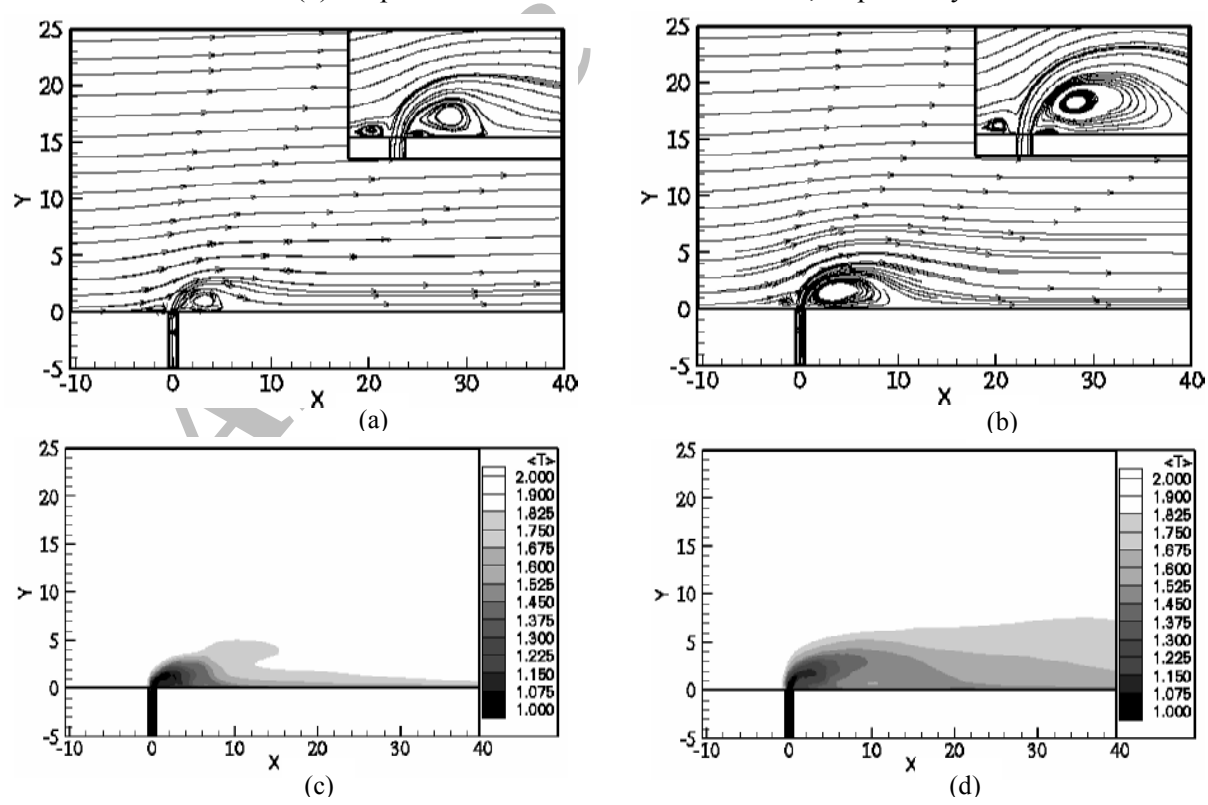

Fig. 6: The flow streamlines and the temperature contours at R=1.5: (a) and (b) Streamlines and (c) and (d) temperature contours at DR=1.0 and 2.0, respectively.

The reattachment point of the downstream vortical region moves approximately 2.1D toward the jet exit. Also, this flow behavior changes the temperature distribution as shown in the temperature contours of Fig. 5. That is, the lower expansion of the downstream vortical region in the X-direction at DR=2.0, results in lower mixing of the cold jet flow with the hot crossflow. Therefore, it is expected to obtain higher film cooling effectiveness by considering the density ratio variations at R=1.0.

In Fig. **6**, the time averaged flow streamlines and the temperature contours are shown for R=1.5 and at DR=1.0 and 2.0. The upstream vortical region contains three vortices at DR=1.0 and one vortex at DR=2.0, while the downstream vortical region contains two vortices at DR=1.0 and three vortices at DR=2.0. By increasing the velocity ratio, the downstream vortical region expands more in Y-direction, but its reattachment point in X-direction decreases at DR=1.0 and increases at DR=2.0. Considering the density ratio variations, the streamlines show that these vortical regions expand more and penetrate deeper into the cross flow in both directions. In contrast to R=0.5 and 1.0, another vortex forms in the upstream vortical region at DR=1.0 and also at the downstream vortical region at DR=2.0. Therefore, by considering the density ratio variations, jet flow penetration into the cross flow in Y-direction increases nearly 1.1D and the reattachment point moves approximately 7.7D outward the jet exit in X-direction. Again, this flow behavior changes the temperature distribution, as shown in the temperature contours of the above mentioned Figure. That is to say, since the reattachment point of the downstream vortical region at DR=1.0 is closer to the jet exit, little mixing of the cold jet flow with the hot crossflow occurs. However, higher penetration of the jet flow in Y-direction causes higher mixing of the two flows at DR=2.0.

Comparing Fig.'s **4**, **5**, and 6, it is observed that penetration of the jet flow into the crossflow in Y-direction increases by increasing the velocity ratio for both cases, which is due to doubling the jet to crossflow momentum ratio. Furthermore, the more dense flow after the jet exit tends to lay over the surface. At each velocity ratio, considering the density ratio variations causes higher penetration except for R=0.5. The reattachment point locations of the separated vortical region after the jet exit for DR=1.0 are 7.2D, 13.8D, and 6.35D. The corresponding velocity ratios, R, for the above mentioned locations are 0.5, 1.0, and 1.5, respectively. However, considering the density ratio variations, the reattachment point locations are 5.6D, 6.35D, and 14.1D for R=0.5, 1.0, and 1.5, respectively.

Figure **7** shows the time averaged turbulent kinetic energy profiles at different velocity ratios for the case of neglecting density ratio variations at different X-locations, namely 0.0, 5.0, 10.0, and 20.0, after the jet exit. It should be noted that, near the jet exit, these profiles show a smooth distribution which rise to a peak away from the wall. The Y-locations of these peaks increase in magnitude with position downstream. Moving away from the jet exit in the cross flow direction, at all velocity ratios, maximum turbulent kinetic energy increases firstly and then decreases and its penetration increases at all. By increasing the velocity ratio, penetration of the turbulent kinetic energy in the cross flow increases and its distribution becomes smoother.

Figure **8** shows the time averaged turbulent kinetic energy profiles at different velocity ratios for the case of considering density ratio variations at different X-locations, namely 0.0, 5.0, 10.0, and 20.0, after the jet exit. By increasing the velocity ratio and/or moving away from the jet exit in the cross flow direction, shape of the turbulent kinetic energy and its penetration show the same behavior as in the case of neglecting density ratio effects. However, by considering the density ratio variations, at all velocity ratios, turbulent kinetic energy penetration increases and would have higher minimum far away from the wall.

To investigate the efficiency of film cooling, a quantity named "adiabatic film cooling effectiveness" is defined as:

$$\eta_{aw} \equiv \frac{T_{aw} - T_{\infty}}{T_{Jet} - T_{\infty}} \qquad (13)$$

where, T_{aw} is the adiabatic wall temperature, T_{Jet} is the cooling air temperature, and T_{∞} is the cross flow temperature. Note that η_{aw} varies between zero having no film cooling, and unity, being cooled to T_{Jet}.

As noted previously, due to the time-dependent behavior of the downstream vortical region, the temperature distribution after the jet exit varies by time at all velocity ratios. Therefore, the film cooling effectiveness would be a function of time, which was time-averaged to obtain a unique profile for each velocity and/or density ratios.

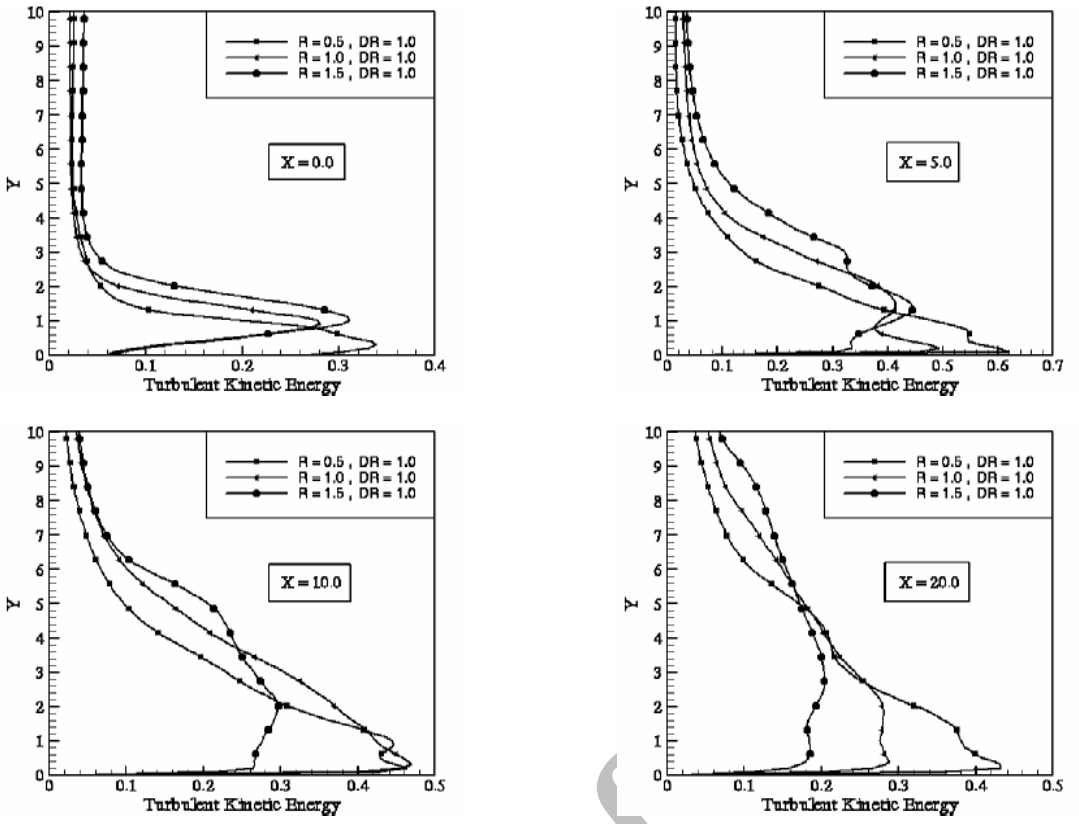

Fig. 7: Time averaged turbulent kinetic energy profiles at different velocity ratios for the case of neglecting density ratio variations at different X-locations after the jet exit.

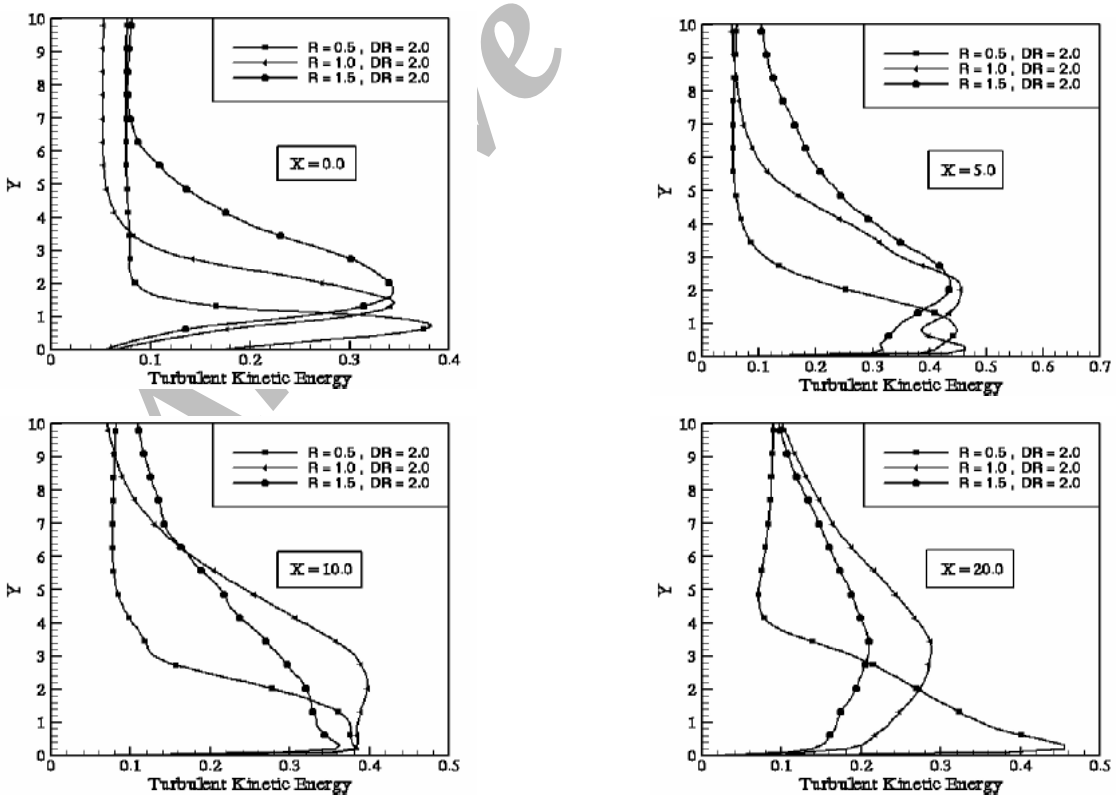

Fig. 8: Time averaged turbulent kinetic energy profiles at different velocity ratios for the case of considering density ratio variations at different X-locations after the jet exit

As noted previously, due to the time-dependent behavior of the downstream vortical region, the temperature distribution after the jet exit varies by time at all velocity ratios. Therefore, the film cooling effectiveness would be a function of time, which was time-averaged to obtain a unique profile for each velocity and/or density ratios. Figure **9** shows the time averaged film cooling effectiveness at different velocity ratios for the case of neglecting the density ratio variations. By increasing the velocity ratio form 0.5 to 1.0 and 1.5, the minimum film cooling effectiveness varies from 0.279, to 0.433 and 0.409, respectively. Also, the space averaged film cooling effectiveness over the surface after the jet exit at X-direction increases from 0.464 to 0.525 and 0.540, respectively.

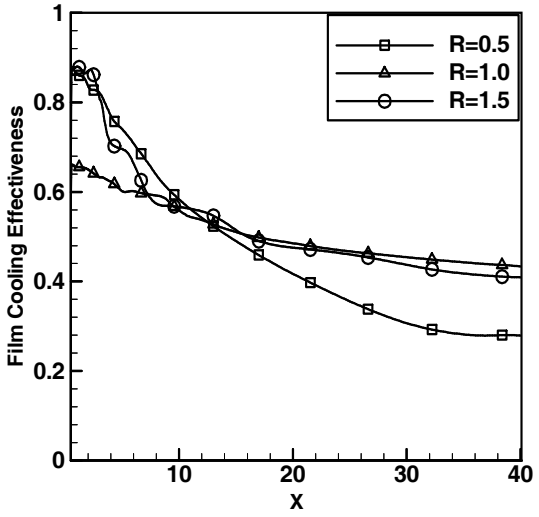

Fig. 9: Time averaged film cooling effectiveness at different velocity ratios for DR=1.0.

Figure **10** shows the time averaged film cooling effectiveness at different velocity ratios for the case of considering the density ratio variations. By increasing the velocity ratio form 0.5 to 1.0 and 1.5, the minimum film cooling effectiveness varies from 0.398, to 0.607 and 0.503, respectively. Also, the space averaged film cooling effectiveness over the surface after the jet exit in X-direction varies from 0.645 to 0.689 and 0.569, respectively.

It should be noted that maximum film cooling effectiveness, physically means that maximum wall cooling is achieved by the cooling jet. Ideally, maximum film cooling effectiveness could be unity, in which, the wall is cooled to the jet temperature. However, minimum film cooling means that minimum wall cooling is performed by the cooling jet. Ideally, minimum film cooling effectiveness could be zero, in which, the wall temperature is equal to the crossflow temperature and no cooling is obtained. The curvature shapes of the lines in Figs. **9** and **10** are due to separation region after the jet exit and the reattachment point of this vortical region.

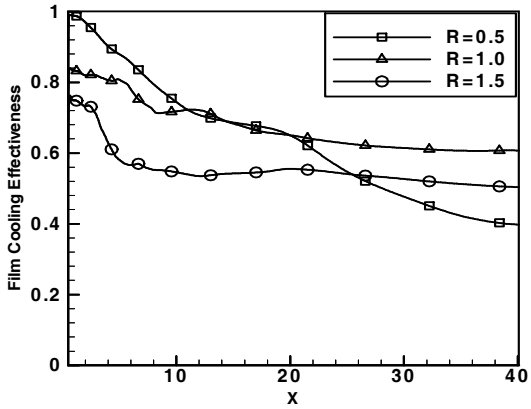

Fig. 10: Time averaged film cooling effectiveness at different velocity ratios for DR=2.0.

Comparing the film cooling effectiveness profiles at the same velocity ratio for both density ratios, it is observed that considering the density ratio variations results in higher film cooling effectiveness. Generally, increasing density ratio increases the jet to crossflow momentum ratio; correspondingly the more dense flow after the jet exit tends to lay over the surface. Therefore, better film cooling effectiveness is obtained. Lower and higher minimum film cooling effectiveness after the jet exit is observed at R=0.5 and 1.0 for both density ratios, respectively. Therefore, in both cases, velocity ratio of 1.0 shows better local film cooling effectiveness. However, higher space averaged film cooling effectiveness is obtained at R=1.5, while neglecting the density ratio variations. Considering the density ratio variations, higher space averaged film cooling effectiveness is obtained at R=1.0. It is concluded that the density ratio variations have significant effects on the flow characteristics, such as penetration, expansion, and reattachment point of the vortical regions. In this regard, the temperature distribution and the film cooling effectiveness varies, which could not be ignored.

6. CONCLUSIONS

Computational simulation was performed at three different velocity ratios, namely, 0.5, 1.0, and 1.5 at the jet Reynolds number of 4700 and at DR=1.0 and 2.0 for the incompressible turbulent flow over a two-dimensional flat plate. Our computational methodology includes the finite volume method, applying unsteady SIMPLE algorithm, and a multi-block and non-uniform staggered grid. The jet is injected normally into the cross flow. The following conclusions are obtained from our investigations:

1. at all considered velocity ratios, there are two separation regions upstream and downstream of the jet exit. In these regions, there are some vortical motions,
2. penetration of the jet flow into the crossflow in Y-direction increases by increasing the velocity ratio for both cases. Also, at each velocity ratio, increasing the density ratio, causes higher penetration except for R=0.5,
3. increasing the velocity ratio, the location of the reattachment point of the separated vortical region after the jet exit moves outward the jet exit,
4. increasing the density ratio increases the jet to crossflow momentum ratio; correspondingly the more dense flow after the jet exit tends to lay over the surface. Therefore, better film cooling effectiveness is obtained,
5. in both cases of neglecting and considering the density ratio, velocity ratio of 1.0 shows better local film cooling effectiveness. However, while neglecting the density ratio, higher space averaged film cooling effectiveness is obtained at R=1.5, and
6. considering the density ratio, higher space averaged film cooling effectiveness is obtained at R=1.0.

References

1. Theodoridis, G.S., Lakehal, D., and Rodi, W., "Three-dimensional Calculations of the Flow Field Around a Turbine Blade with Film Cooling Injection Near the Leading Edge", J. Flow, Turbulence and Combustion, Vol. 66, No. 1, pp. 57-83, 2001.
2. Ardey, S., "3D-Messung des Stromungsfeldes um die Filmgekuhlte Vorderkante einer Referenzschaufel", Abschlussbericht zum TURBOTHERM II-Verbundvorhaben 2.1.8.4 der Arbeitsgemeinschaft Hochtemperatur Gasturbine, Bericht LTR-Inst., 12-98/02, Universitat der Bundeswher Munchen., 1998.
3. Bergeles, G., Gosman, A.D., and Launder, B.E., "The Turbulent Jet in a Cross Stream at Low Injection Rates: A Three-dimensional Numerical Treatment", Numerical Heat Transfer, Vol. 1, pp. 217-242, 1978.
4. Lin, Y.L. and Shih, T.I.P., "Film Cooling of a Cylindrical Leading Edge with Injection Through Rows of Compound-angle Holes", J. Heat Transfer, Vol. 123, No. 4, pp. 645-654, 2001.
5. Azzi, A. and Lakehal, D., "Perspectives in Modeling Film Cooling of Turbine Blades by Transcending Conventional Two-equation Turbulence Models", J. Turbomachinery, Vol. 124, No. 3, pp. 472-484, 2002.
6. Roy, S., Kapadia, S., and Heidmann, J.D., "Film Cooling Analysis, Using DES Turbulence Model", GT-2003-38140, Atlanta, Georgia, USA., 2003.
7. Ramezanizadeh, M., "Large Eddy Simulation of Film Cooling in a Turbulent Flow Over a Flat Plate", M.Sc. Thesis, Aerospace Engineering Department, Sharif Univ. of Tech., Tehran, Iran, 2000.
8. Ramezanizadeh, M. and Taeibi-Rahni, M., "Large Eddy Simulation of Multiple Jets in a Cross Flow, Using Smagorinsky Model", ISME 2001, Guilan University, Rasht-Iran, pp. 293-299., 2001.
9. Keimasi, M.R. and Taeibi-Rahni, M., "Numerical Simulation of Jets in a Crossflow, Using Different Turbulence Models", AIAA J., Vol. 39, No. 12, pp. 2268-2277, 2001.
10. Ramezanizadeh, M. and Taeibi-Rahni, M., "Large Eddy Simulation of a Two-dimensional Flat Plate Film-Cooling", The 9th Asian Congress of Fluid Mechanics, Isfahan, Iran, 2002.
11. Ramezanizadeh, M., Saidi, M.H., and Taeibi-Rahni, M., "Large Eddy Simulation of Density Ratio Effects on Two-dimensional Film Cooling", The 2nd BSME-ASME Int. Conf. on Thermal Eng., Vol. 2, pp. 659-665, Dhaka, Bangladesh., 2004.
12. Spyropoulos, E.T. and Blaisdell, G.A., "Large-Eddy Simulation of a Spatially Evolving Supersonic Turbulent Boundary–Layer Flow", AIAA J., Vol. 36, No. 11, pp. 1983-1990, 1998.
13. Peyret, R., "Handbook of Computational Fluid Mechanics", Academic Press, San Diego., 1996.
14. Tafti, D. K., Zhang, X., Huang, W., and Wang, G., "Large-Eddy Simulations of Flow and Heat Transfer in Complex Three-dimensional Multilouvered Fins", FEDSM2000-11325, Boston, Massachusetts, USA, 2000.
15. Zhang, W. and Chen, Q., "Large Eddy Simulation of Indoor Airflow with a Filtered Dynamic Subgrid Scale Model", Int. J. Heat and Mass Transfer, Vol. 43, pp. 3219-3231, 2000.
16. Peng, S.H. and Davidson, L., "Comparison of Subgrid-Scale Models in LES for Turbulent Convection Flow with Heat Transfer", The 2nd Turbulent Heat Transfer Conf., Manchester, UK, Vol. 1, pp. 5.25-5.35., 1998.
17. Ajersch, P., Zhou, J.M., Ketler, S., Salcudean, M., and Gartshore, I.S., "Multiple Jets in a Crossflow: Detailed Measurements and Numerical Simulations", Int. Gas Turbine and Aeroengine Congress and Exposition, Houston, Texas., 1995.

18. Ghia, U., Ghia, K.N., and Shin, C.T., "High-Resolution for Incompressible Flow, Using the Navier-Stokes Equations and a Multigrid Method", J. Comp. Phys., Vol. 48, pp. 387-411, 1982.
19. Prasad, A.K. and Koseff, J.R., "Reynolds Number and End-Wall Effects on a Lid-Driven Cavity Flow", Phys. Fluids A, Vol. 1, pp. 208-218, 1989.
20. Taeibi-Rahni, M. and Ramezanizadeh, M., "Investigation of Three-dimensional Cavity Flow, Using Large Eddy Simulation Approach", Journal of Aerospace Science and Technology, Iranian Aerospace Society, Vol. 2, No. 2, pp. 1-10., 2005